Laser-induced periodic surface structures on P3HT and on its photovoltaic blend with $PC_{71}BM$

*Jing Cui[1], Álvaro Rodríguez-Rodríguez[1], Margarita Hernández[1], Mari-Cruz García-Gutiérrez[1], Aurora Nogales[1], Marta Castillejo[2], Daniel Moseguí González[3], Peter Müller-Buschbaum[3], Tiberio A. Ezquerra[1] and Esther Rebollar[2]**

[1] Instituto de Estructura de la Materia (IEM-CSIC), Serrano 121, 28006 Madrid, Spain.

[2] Instituto de Química Física Rocasolano (IQFR-CSIC), Serrano 119, 28006 Madrid, Spain.

[3] Lehrstuhl für Funktionelle Materialien, Physik-Department, Technische Universität München, James-Franck-Str. 1, 85748 Garching , Germany

*Corresponding author: e.rebollar@csic.es

KEYWORDS: laser induced periodic surface structures, polymer films, semiconductor polymers, grazing incidence x-ray scattering, organic photovoltaics

ABSTRACT

We describe the conditions for optimal formation of Laser Induced Periodic Surface Structures (LIPSS) over poly(3-hexylthiophene) (P3HT) spin-coated films. Optimal LIPSS on P3HT are

observed within a particular range of thicknesses and laser fluences. These conditions can be translated to the photovoltaic blend formed by the 1:1 mixture of P3HT and [6,6]-phenyl C_{71}-butyric acid methyl ester ($PC_{71}BM$) when deposited on an indium tin oxide (ITO) electrode coated with (poly(3,4 – ethylenedioxythiophene) : poly(styrenesulfonate) (PEDOT:PSS). Solar cells formed by using either a bilayer of P3HT structured by LIPSS covered by $PC_{71}BM$ or a bulk heterojunction with a P3HT:$PC_{71}BM$ blend structured by LIPSS exhibit generation of electrical photocurrent under light illumination. These results suggest that LIPSS could be a compatible technology with organic photovoltaic devices.

1. INTRODUCTION

Several materials are being investigated as alternative candidates to the well-established silicon solar cells. Among them organic photovoltaics (OPV) involve the use of π-conjugated semiconducting polymers for light absorption and charge transport[1-6]. Polymer blends and inorganic/organic hybrid solar cells have attracted a great interest due to their potential in combining the advantages of both components [7-10]. In particular polymer-fullerene mixtures of poly(3-hexylthiophene) (P3HT) with [6,6]-phenyl C_{61}-butyric acid methyl ester ($PC_{61}BM$) or [6,6]-phenyl C_{71}-butyric acid methyl ester ($PC_{71}BM$) have been widely used as model system in organic photovoltaics (OPV) [4, 5, 11-17], despite other material combinations have reached meanwhile much higher power conversion efficiencies [18-21]. In general, the interfacial area between the donor material, P3HT, and the acceptor one, either $PC_{61}BM$ or $PC_{71}BM$, which form the heterojunction, is a critical factor for the performance of the OPV devices [11, 22]. OPVs can be fabricated by different techniques, such as spin coating, spray deposition, vapor phase deposition and printing[23-26]. The

modification of the photoactive layer with periodic structures has been extensively studied recently because it can be an effective way to improve light harvesting[27]. In particular, several approaches have been followed in order to fabricate controlled P3HT micro- and nanostructures for OPV applications including soft lithography [27], nanoimprint lithography [28-30], templating by anodic aluminium oxide (AAO) membranes [31], solvent annealing [11, 32], and spray deposition [33], among others. Laser techniques in general and Laser-Induced Periodic Surface Structures (LIPSS) [34] in particular can be considered potential alternatives to other lithography processes, with the added advantage of avoiding, in principle, the need for sophisticated facilities like clean rooms or the fabrication of delicate stamps. Ripples created by LIPSS can develop on the polymer surface as a result of interference between an incoming linearly polarized laser beam and the surface-scattered waves which results in a heterogeneous light intensity distribution on the surface [35]. Irradiation with multiple laser pulses enhances the effect by a feedback mechanism that is needed for LIPSS generation [35, 36]. The ripple period depends on the laser wavelength, on the effective refractive index of the material and on the incidence angle of the laser beam [34]. Either nanosecond [37] or femtoseconds lasers [38] can be used to produce LIPSS on polymers. In particular LIPSS have been used in order to create sub-micron gratings on P3HT [36]. It was shown that, in spite of the well-known photodegradability of P3HT and of the high power of the laser pulses applied, LIPSS on this material obtained with a wavelength of 532 nm are produced with a weak impact on its chemical structure. However the electrical conductivity of the rippled P3HT films exhibits a heterogeneous nature consisting of the alternation of conducting valleys and non-conducting hills [36]. On the basis of Raman spectroscopy and of X-ray scattering measurements, a reduction of the crystallinity of the hills was proposed as the cause of these effects [36]. From the perspective of OPV, several questions arise about the potential integration of P3HT LIPSS in solar cell architectures [39,

[40]. These include: 1) the possibility of creating LIPSS on an active layer comprising P3HT and $PC_{71}BM$, 2) the feasibility of intercalation of the LIPSS active layer between a bottom ITO electrode coated with a thin layer of poly(3,4-ethylenedioxythiophene):poly(styrenesulfonate) (PEDOT:PSS) and a metallic top electrode and 3) the impact of the heterogeneous electrical conductivity of the P3HT LIPSS surface on the OPV device properties.

Thus, the novelty of this work is the attempt to provide some answers to the above-mentioned questions by presenting a precise description of LIPSS formation in P3HT spin-coated films of variable thickness. Once the conditions for optimal LIPSS formation were found we created LIPSS on P3HT:$PC_{71}BM$ blends for their potential integration in solar cell architectures. Due to the fact that irradiation of a conjugated polymer, extremely photodegradable, by intense laser pulses leaves the polymer capable of generating photocurrent is not a trivial aspect, we have used the LIPSS nanostructured films to prepare solar cells devices and their performance has been measured and compared with that of the non-structured counterparts.

2. EXPERIMENTAL

2.1 Poly(3-hexylthiophene) thin films

Poly(3-hexylthiophene) (P3HT) was purchased from Ossila with a molecular weight M_w= 65.500 g/mol (Batch M101, tradename lisicon®, regioregularity of 96.6%). Thin polymer films were prepared by spin-coating using a spin processor (Laurell WS-650 Series). The conductive silicon wafers (100) (ACM, France) were cut into pieces of 2×2 cm^2, cleaned by acetone and 2-propanol and then dried under Nitrogen flow. A P3HT polymer solution in chloroform was prepared with a concentration of 32 g/L and was stirred at room temperature for 30 min. A fixed amount of 0.2 mL of solution was spun coated on silicon wafers at a rotation rate of 2400 rpm kept

during 120 s. Different film thicknesses were obtained by diluting the initial solution. Both thickness and roughness of the obtained thin films were estimated by Atomic Force Microscopy (AFM).

2.2. Laser irradiation

Laser irradiation was accomplished under atmospheric conditions and normal beam incidence by using a linearly polarized beam from a Q-switched Nd:YAG laser (Lotis TII LS-2131M, pulse duration of 8 ns). The second harmonic (532 nm) was used for the experiments since P3HT absorbs quite efficiently at this wavelength[41], being its absorption coefficient ~ 9 x 10^4 cm^{-1} as determined by absorption spectroscopy using a UV-VIS-NIR spectrophotometer (UV-3600 Shimadzu). The irradiation fluences were determined by measuring the laser energy in front of the sample with a Joulemeter (Gentec-E, QE25SP-H-MB-D0) and by calculating the area of the irradiated spots, considering 5 mm as the diameter of the laser beam. P3HT films were irradiated with 3600 pulses at a fluence in the range from 23 to 31 mJ/cm^2, at a constant repetition rate of 10 Hz for all samples. A general description of the application of this technique to polymers has been published elsewhere[34].

2.3. Sample characterization

2.3.1. Atomic Force Microscopy

Atomic Force Microscopy (AFM) (MultiMode 8 equipped with a Nanoscope V controller, Bruker) was used under ambient conditions in order to investigate the topography of the samples. AFM images were collected in tapping mode using silicon probes (NSG30 probes by NT-MDT). Heights and periods were measured in 3 different zones of the sample to examine the film uniformity. Analysis of images was carried out using Nanoscope Analysis 1.50 software (Bruker).

2.3.2. Grazing Incidence X-ray Scattering

Grazing Incidence Small and Wide Angle X-ray Scattering (GISAXS, GIWAXS respectively) experiments were performed at the DUBBLE beamline of the European Synchrotron Radiation Facility (ESRF, Grenoble, France) [36, 42]. A X-ray wavelength of 0.103 nm, with a beam size (Horizontal ×Vertical) of 0.7 × 0.3 mm^2 was employed. To acquire GISAXS patterns, the samples were placed with its surface horizontal and parallel to the X-ray beam and at a height which intercepted half of the beam intensity. The sample was then tilted to reach different incidence angles between the sample surface and the beam. In our case, incidence angles of 0.14º, 0.2º, 0.3º and 0.4º were used to obtain information at different depths of the film. GISAXS patterns were acquired with a Pilatus detector of 981 × 1043 pixels, pixel size 172 x 172 μm^2, located at 7.2 m from the sample. The exposition time was set 5 s. For GIWAXS measurements, the scattered intensity was recorded by a Frelon detector of 2048 × 2048 pixels with a resolution of 46.8 μm per pixel, with a sample-detector distance of 79.32 mm. Patterns acquired with an exposition time of 10 s were corrected from background scattering and analyzed by the Fit2D software [43].

2.3.3. Preparation of P3HT:$PC_{71}BM$ solar cells

For preparation of organic solar cells, solutions of P3HT (Ossila, M_w= 34100 g/mol, PDI= 1.7, regioregularity= 94.7%) and $PC_{71}BM$ (Ossila, UK) were prepared in chlorobenzene (24 g/L). The molecular weight of P3HT and the chlorobenzene as solvent were chosen in order to allow comparison with previous studies [36]. A thin layer of PEDOT:PSS (poly(3,4-ethylene dioxythiophene): poly(styrenesulfonate), Heraeus Clevios™ PH1000 PEDOT:PSS, Ossila [39] was deposited by spin-coating at 5000 rpm on top of ITO-covered glass substrates (Solems S.A, France). Two different solar cell architectures were prepared for the P3HT:$PC_{71}BM$ active layer: 1) A bilayer was formed by depositing a P3HT layer spin-coated at 2400 rpm for 120 s on the

underlying PEDOT:PSS layer and subsequently covered by another $PC_{71}BM$ layer spin coated at 4000 rpm for 10 s from a 5 mg/mL dichloromethane solution. 2) A bulk heterojunction (BHJ) active layer formed by the P3HT:$PC_{71}BM$ blend (weight ratio of 1:1) spin-coated over the PEDOT:PSS film at 2400 rpm for 120 s. Afterwards, in both cases, an aluminium top electrode was deposited by thermal evaporation in vacuum [22]. Finally, a thermal annealing step of 4 minutes at 140^{o} C was performed in a glove box under N_2 atmosphere. The photovoltaic devices were characterized at ambient conditions under the AM 1.5 global reference spectrum and 100 mW cm^{-2} irradiance. The current–voltage measurements were recorded using a source meter (Keithley 2400).

3. RESULTS AND DISCUSSION

3.1. LIPSS in P3HT thin films

Figure 1 shows the thickness dependence of the spin-coated (SC) P3HT films with the solution concentration. A linear relationship is observed in good agreement with earlier reports [44-46]. The upper row in Figure 1 shows AFM topography images of SC P3HT films of selected solution concentrations covering the full range of film thicknesses investigated.

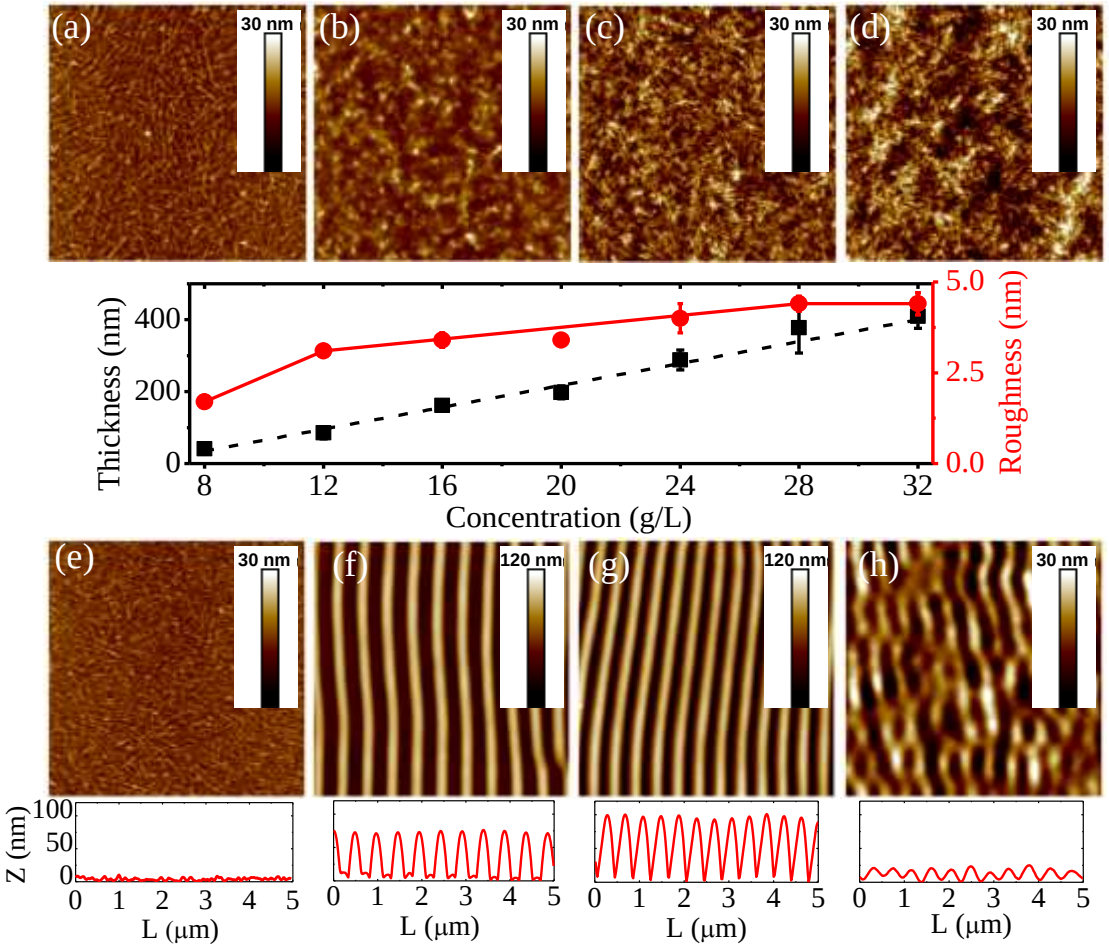

Figure 1. Thickness (squares) and roughness (circles) dependence of the SC P3HT films on the solution concentration (middle row). Selected AFM topography images (5×5 μm^2) of SC P3HT (upper row) films before irradiation prepared from (a) 8 (b) 12 (c) 20 and (d) 28 g/L, and after irradiation at a fluence of 26 mJ/cm^2 with 3600 pulses from (e) 8 (f) 12 (g) 20 and (h) 28 g/L. The height profiles (depth, Z, versus distance, L) of irradiated SC P3HT films are presented under the corresponding AFM images.

The as-prepared SC films present the characteristic morphology of semicrystalline P3HT consisting of needle crystals [47, 48]. The roughness of the SC films increases with thickness, levelling

off for thicker samples. LIPSS formation in these films depends on thickness as exemplified by the bottom row in Figure 1. While, under the same irradiation conditions (26 mJ/cm^2, 3600 pulses), thin films of ≈ 41 ± 15 nm (Figure 1e) do not exhibit LIPSS, those with intermediate thicknesses, in the range of ca. 80-280 nm (Figure 1 f and g) present a regular periodic relief with a period of ca. 430 nm. It is known that when a polymer film is irradiated with a linearly polarized laser beam at an efficiently absorbed wavelength, the nanosecond laser pulses heat the material surface driving the polymer above either its glass transition temperature, for the case of an amorphous polymer, or above its melting point, in case of a semicrystalline polymer [34, 37]. This is a requisite for LIPSS formation in polymers since significant molecular dynamics is necessary in order to allow LIPSS to generate [37, 49]. In general, thinner films need more irradiation energy, in terms of either number of pulses or fluence, in order to reach similar temperatures than those reached by thicker films[50, 51]. Specifically, for silicon substrates, the laser irradiation of the polymer film provokes the substrate temperature to increase very fast. However, the heat is effectively dissipated on the basis of the high thermal diffusivity of silicon. Thus, the high thermal conductivity and thermal diffusivity of silicon makes the cooling of the polymer material heated by the laser pulse to be more efficient for thinner films. Accordingly, the silicon substrate acts as a thermal heat sink. Although in the thicker investigated films LIPSS are formed (Figure 1 h), these are significantly distorted in comparison with those generated in films of intermediate thickness. For these thicker films, in a first approach, roughness may play a significant role on the quality of LIPSS producing complex light scattering processes on the sample surface leading to non-parallel interferences.

GISAXS measurements have proven to be useful for the characterization of structural order in LIPSS formed over polymer films as it provides statistical information integrated over a large sample area of the material surface [36, 37, 49]. Figure 2 shows a series of GISAXS patterns of

irradiated films as a function of the concentration. The measurements were performed with an incidence angle of $\alpha_i = 0.2$ °.

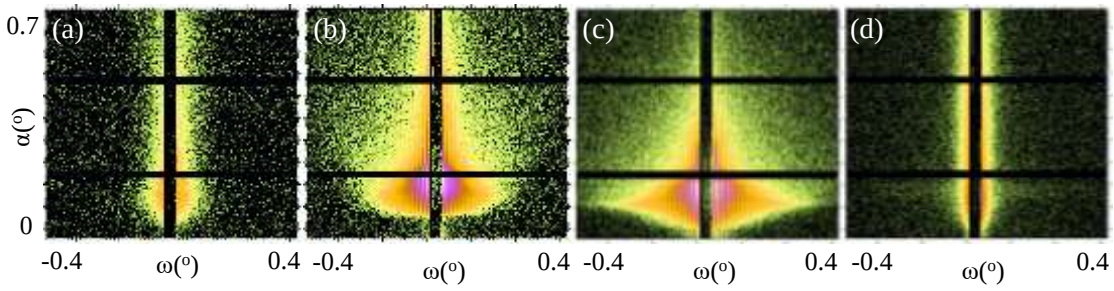

Figure 2. GISAXS patterns taken with an incidence angle of α_i =0.2° for P3HT LIPSS films prepared from (a) 8 (b) 12 (c) 20 and (d) 28 g/L solutions with LIPSS generated at a fluence of 26 mJ/cm^2 with 3600 pulses. A central vertical beamstop is used to avoid oversaturation of the detector. The horizontal black lines are the detector inter-module gaps.

For the thinner (8 g/L, 41 ± 15 nm, Figure 2a) and thicker (≥ 28 g/L, ≥ 370 nm, Figure 2d) irradiated P3HT films the scattering patterns show the same characteristic scattering features as those of unstructured spin coated films as there is an absence of relevant structure in the angular range investigated [36]. On the contrary, GISAXS patterns of the intermediate thickness films (12-20 g/L, 80-280 nm, Figures 2b and c) exhibit vertical diffraction maxima out of the meridian ($\omega \neq 0$) typical of LIPSS as previously reported[36, 37, 49]. These features can be described as produced by a quasi-one-dimensional grating [52]. Figure 3 shows horizontal line cuts from the 2D GISAXS data at $\alpha_i = 0.2$ ° taken at an exit angle $\alpha = 0.15$ ° which corresponds to the experimentally estimated critical angle of P3HT. While the intensity profiles for the thinner and thicker irradiated films are featureless, those of the films with intermediate thickness show vertical diffraction maxima. It is observed that the number of the scattering maxima (*N*) increases with the concentration, i.e. film

thickness. The number of scattering maxima, which is associated to the structure factor of the lattice [52], is related to the level of order of the structure [36]. The inset of Figure 3 shows the thickness dependence of the number of scattering maxima observed in the GISAXS pattern. It is clear that LIPSS films prepared from solutions with polymer concentration between 16 g/L and 20 g/L are those exhibiting richer GISAXS patterns in terms of the number of scattering maxima. These results are in agreement with the AFM images (Figure 1) which reveal that optimal LIPSS, understood as those with a higher order, appear within this polymer solution concentration range.

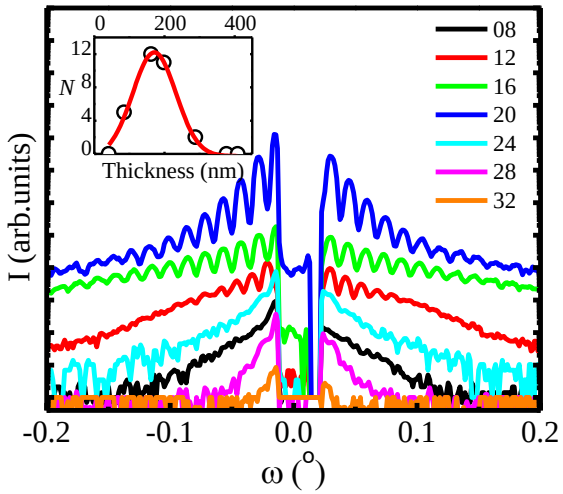

Figure 3. Selected horizontal line cuts in logarithmic scale from the 2D GISAXS data taken at an exit angle α=0.15 º, for LIPSS generated at 26 mJ/cm^2 with 3600 pulses on P3HT films prepared from different solution concentrations (g/L) as labelled. Patterns were shifted vertically for the sake of comparison. The inset displays the number of scattering maxima (*N*) obtained from GISAXS as a function of thickness. The continuous line is a guide for the eye.

The semicrystalline nature of P3HT as well as of most poly(alkylthiophene) polymers [53, 54] is a key feature of their film morphology and plays a capital role in the performance of a posterior

organic solar cell. Therefore, characterization of the effect of LIPSS treatment on the crystallinity of P3HT:PCBM films provides greater insight on polymer film solar cell-relevant features. Figure 4 shows GIWAXS patterns illustrating the evolution of the structure of P3HT SC films before and after generation of LIPSS with solution concentration. It is known that quantitative analysis of GIWAXS patterns requires a thorough knowledge of the scattering pattern in the reciprocal space [55, 56]. The real to reciprocal space transformation has been accomplished according to the procedure described in ref. [57]. In this case, the intensity of the GIWAXS scattering patterns are represented as a function of the reciprocal scattering vectors q_z and of $q_R = \sqrt{q_x^2 + q_y^2}$ where q_x, q_y and q_z are the scattering vectors.

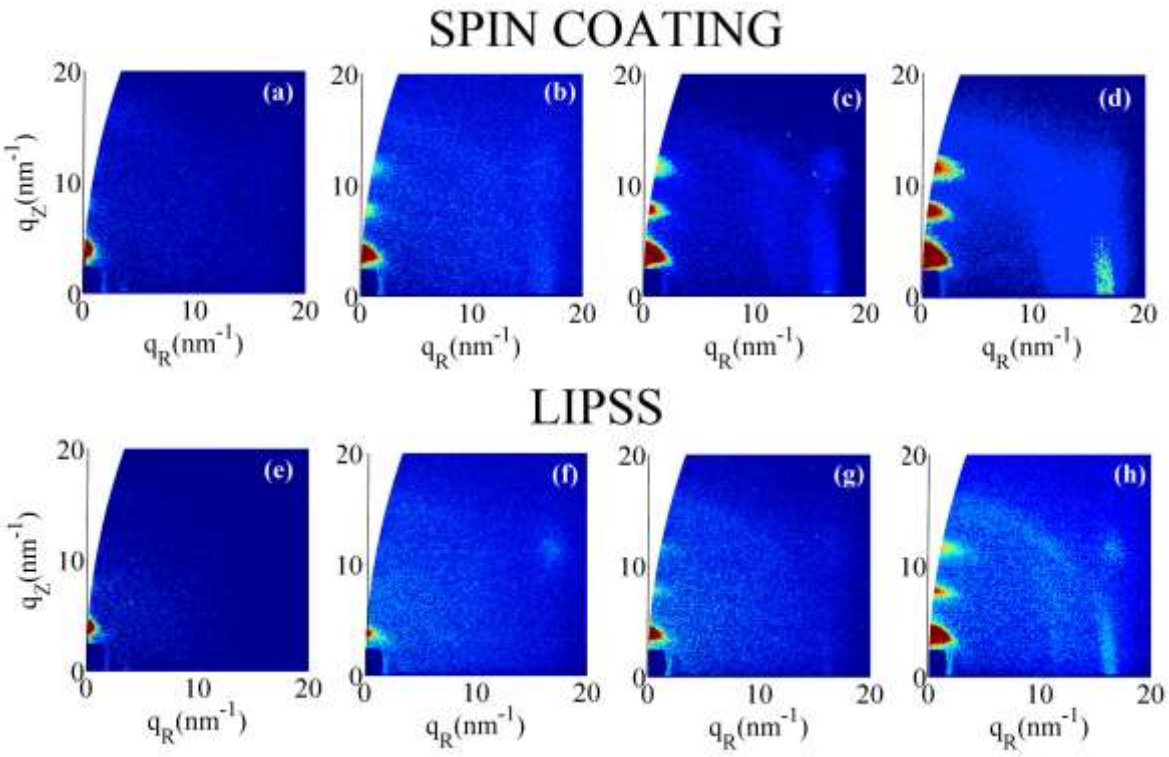

Figure 4. GIWAXS patterns in reciprocal space taken with an incidence angle α_i =0.2° for the SC P3HT films prepared from different solution concentrations: (a) 8 (b) 12 (c) 20 and (d) 28 g/L (upper row) and corresponding irradiated P3HT films (26 mJ/cm^2, 3600 pulses) prepared from

different solution concentrations: (e) 8 (f) 12 (g) 20 and (h) 28 g/L (bottom row). Intensity scale is logarithmic.

The SC films exhibit the characteristic three meridional reflections (h00) of the crystalline phase of P3HT which are higher orders of the (100) reflection (Figure 4a-d). The equatorial reflection is attributed to the superposition of the (020) and (002) reflections [58, 59]. These GIWAXS patterns are in agreement with previous studies reporting a crystal distribution of P3HT sheets formed by the π–π stacking of the thiophene rings on a mainly edge-on configuration, with polymer backbone chains parallel to the substrate [59]. P3HT films with LIPSS exhibit similar reflections as observed in Figure 4e-h. In addition, in our case, by visualizing of the reciprocal space patterns for the different samples a significant crystal orientation is suggested. The interlayer distance between 2D sheets of conjugated polythiophene backbones separated by planes of alkyl side chains has been calculated in 1.58 ± 0.02 nm and 1.60 ± 0.03 nm for unstructured and LIPSS films respectively, and the the π–π stacking distance between polythiophene backbones is 0.38 ± 0.02 nm in both cases. These results are in agreement with previous reports[58, 59]. Qualitative information about the crystallinity can be obtained by the radial integration of the GIWAXS pattern in the meridian direction shown in Figure 5. For the sake of comparison, the data have been normalized to the intensity of the main maximum.

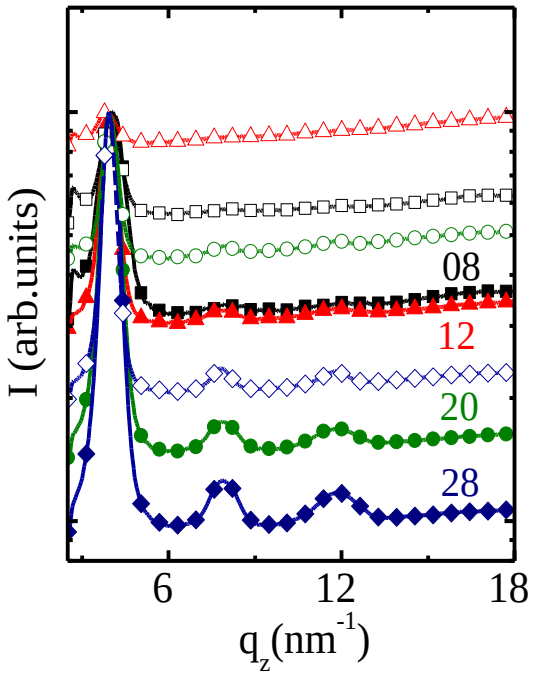

Figure 5. GIWAXS (α_i =0.2°) intensity profiles, normalized to the main maximum, across the meridian direction for the SC P3HT films (solid symbols) and for the laser irradiated films (open symbols) prepared from different solution concentrations: 8, 12, 20 and 28 g/L, as labelled.

From Figure 5, we can find that the crystalline structure is similar for non-nanostructured P3HT and for P3HT with LIPSS films. If one considers the intensity ratio among the consecutive maxima, it is possible to infer that the crystallinity of the SC films tends to be reduced as the thickness of the film decreases. Crystallization under the confined environment imposed by a thin film has been reported to have a negative impact on the crystallinity of the polymer film [47, 60, 61]. Although films with LIPSS exhibit crystallinity it is clear that the irradiation reduces the crystalline phase, as deduced from the decrease of the ratio between the intensity of the main maximum in relation to the consecutive orders. This effect is consistent with previous resonance Raman

spectroscopy observations indicating that the amount of non-ordered phase in P3HT films with LIPSS increases upon irradiation [36]. Heating due to laser irradiation occurs in a nanosecond range while subsequent cooling down after the pulse action takes place in a millisecond time range [37] . This fast quenching prevents the recovery of the initial crystallinity of the SC film.

All the results presented so far refer to films with LIPSS prepared at a single fluence of 26 mJ/cm^2 and 3600 pulses. LIPSS films have been prepared in a broader range of fluences keeping the same number of pulses in order to study comprehensively the effect of laser fluence on the resulting structure. Figure 6a and 6b show in a 3D plot the surfaces defining the period (Figure 6a) and the depth (Figure 6b) of the LIPSS obtained from AFM measurements as a function of the fluence for the different thicknesses investigated. For the thinnest films, no LIPSS are formed (see Figure 1e). As argued before, this phenomenon is ascribed to the fact that thin films need more irradiation for achieving a certain aim temperature. As one can see, once the LIPSS are generated on the P3HT film, their period is almost constant around a value of 430 nm for all the investigated thicknesses (Figure 6a). This would, in principle, allow for keeping laser fluences low, which eventually would have a positive impact on the later device performance. However, as depicted in Figure 6b, the choice of the laser fluence is mainly limited by the LIPSS depth. The depth of the LIPSS exhibits a clear dependence with both the irradiation fluence and the initial thickness of the spin-coated precursor film. Deeper LIPSS are obtained for films thicknesses between 100 and 250 nm, with values up to 100 nm. This thickness range corresponds to the region of optimal LIPSS formation according to AFM (Figure 1) and GISAXS (Figure 2). Within this thickness range, we observe that the required laser fluence for a structure depth of over 80 nm is somewhat confined between 25 and 30 mJ/cm^2. For thicker films the depth of the obtained LIPSS decreases to few nanometers. The absence of structure in thick films is also in excellent agreement with the

previously presented GISAXS data and it is ascribed to the influence of the large film roughness on the quality of interference formation.

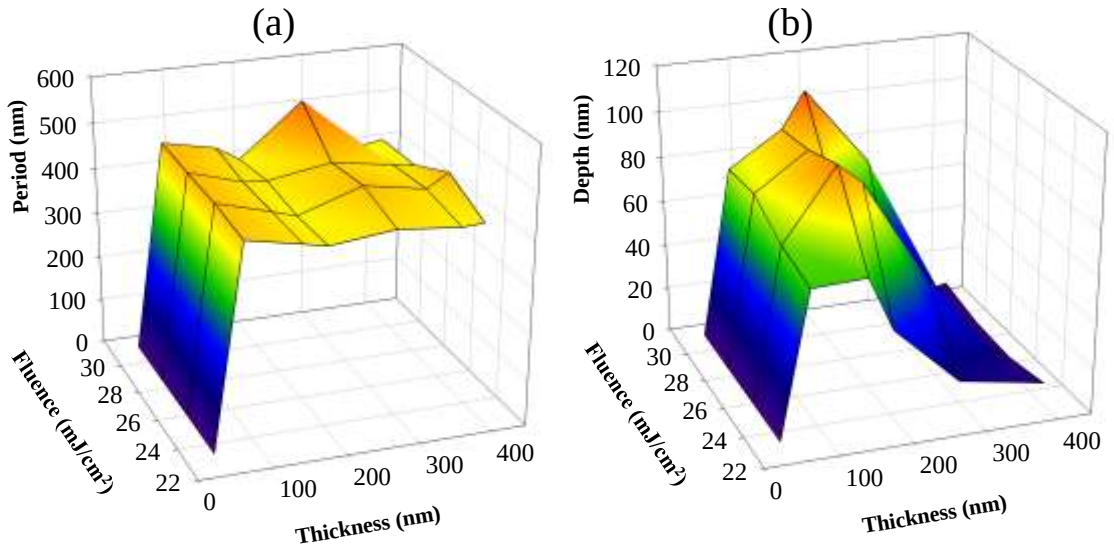

Figure 6. 3D plots showing the surfaces defining the period (a) and depth (b) of LIPSS generated in P3HT films with 3600 pulses as a function of the fluence for the different thicknesses investigated.

Since the formation of LIPSS in P3HT spin-coating films has been successful we apply this knowledge to incorporate LIPSS technology in polymer solar cells.

3.3. LIPSS in P3HT and in P3HT:$PC_{71}BM$ blend for photovoltaics

As mentioned before, for photovoltaics characterization both bilayer and standard bulk heterojunction solar cells [39] were prepared. In both cases the thickness of the active layer is about 110 ± 10 nm as measured by AFM. According to the LIPSS study on P3HT films, the laser selected conditions for LIPSS formation were 3600 pulses of 26 mJ/cm^2. We used these conditions for both architectures, as described in paragraph 2.3.3.

Figure 7a shows a scheme of the bilayer device architecture approach. Also for this device architecture LIPSS appear on P3HT after appropriate laser irradiation conditions as shown in Figure 7b. The upper surface of the $PC_{71}BM$ film spin-coated over the P3HT film with LIPSS is shown in Figure 7c, where the LIPSS imposed on P3HT are maintained. The final deposition of aluminium top contacts by thermal evaporation keeps as well the LIPSS relief essentially unchanged (Figure 7d) with only a slight modification of the depth profile. An example of the I-V characteristics of the LIPSS solar cell in the dark and under illumination is shown in Figure 7e. Although the overall device performance can be optimized, the I-V characteristic of the LIPSS bilayer proves that photocurrent is generated by light illumination. Since also the reference P3HT:PCBM solar cells without LIPSS show very limited performance, it is obvious that the bilayer device geometry is not optimized. Moreover, polymer:fullerene solar cells in bilayer configuration tend to yield rather poor efficiency values due to the small interface between donor and acceptor phases.

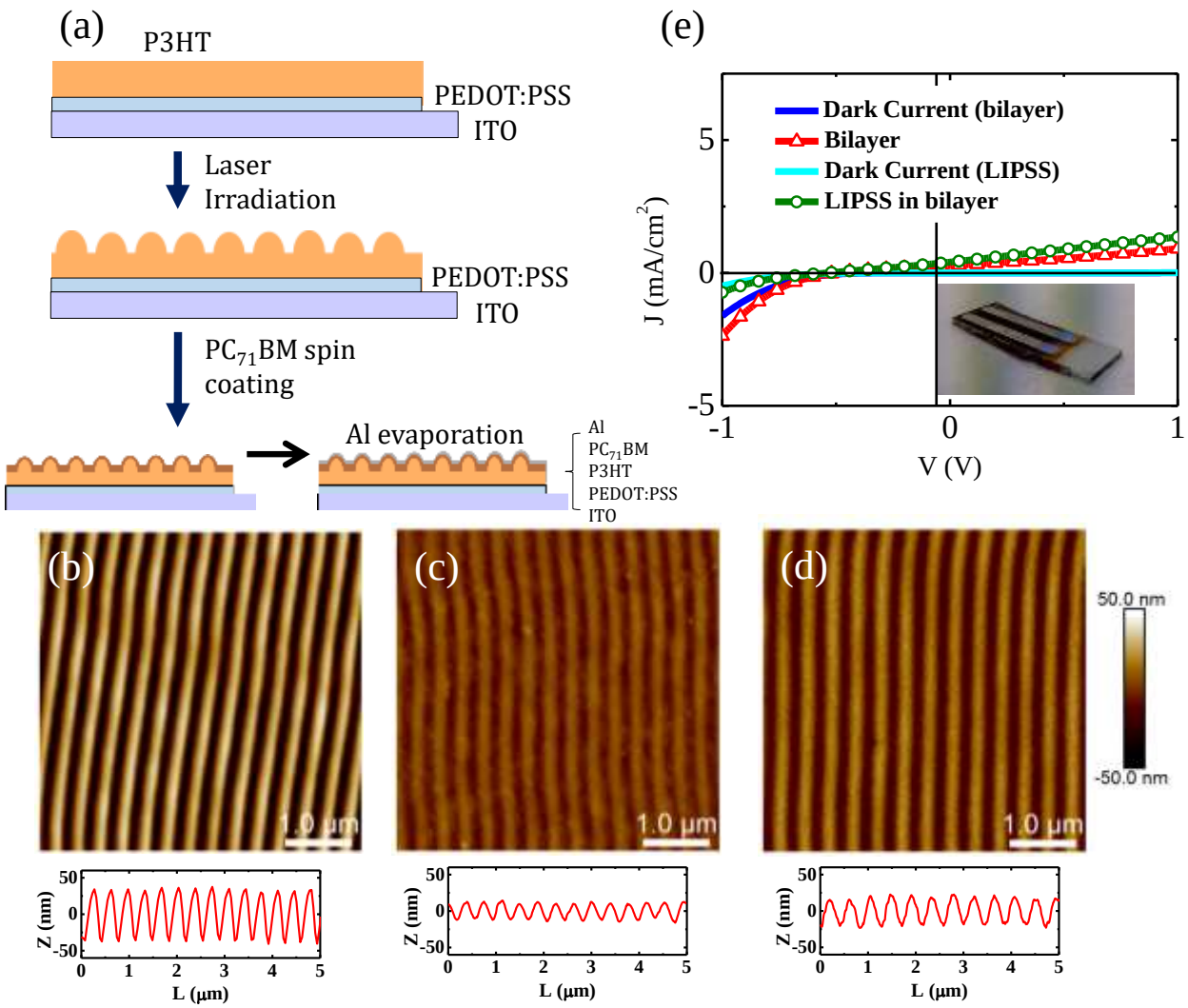

Figure 7. (a) Scheme of the bilayer device architecture tested for photovoltaic characterization of P3HT and $PC_{71}BM$ systems with LIPSS. 5x5 μm^2 AFM images of bilayer solar cell: (b) P3HT surface after laser irradiation and (c) $PC_{71}BM$ film surface deposited on top of P3HT film with LIPSS by spin coating. (d) Surface after deposition of the aluminium top electrode. Height profiles are provided at the bottom of the images. (e) I-V characteristics of the LIPSS solar cell in the dark and under illumination. For the sake of comparison, data for the unstructured bilayer solar cell are also included). The inset in Figure 7e shows the real bilayer solar cell device. The blue color corresponds to the iridescence of the LIPSS area acting as a diffraction grating.

The corresponding results for the bulk heterojunction solar cells (see scheme in Figure 8a) are illustrated in Figure 8. The upper surface of the initial spin-coated P3HT:$PC_{71}BM$ film is shown before (Figure 8b) and after laser irradiation (Figure 8c). It is important to point out that even after thermal annealing LIPSS keep their structure unchanged, at least under the aluminium electrode (see iridescence in the inset of Figure 8e and Figure 8d). As one can see, similarly as for P3HT, rather ordered LIPSS are formed even for the P3HT:$PC_{71}BM$ photovoltaic blend film on the architecture of the standard BHJ solar cell. As an example the I-V characteristics of the BHJ LIPSS solar cell in the dark and under illumination is shown in Figure 8e. The I-V characteristic of the LIPSS heterojunction also proves that photocurrent is generated by light illumination although a lower photocurrent is generated in comparison with the unstructured control bulk heterojunction solar cell.

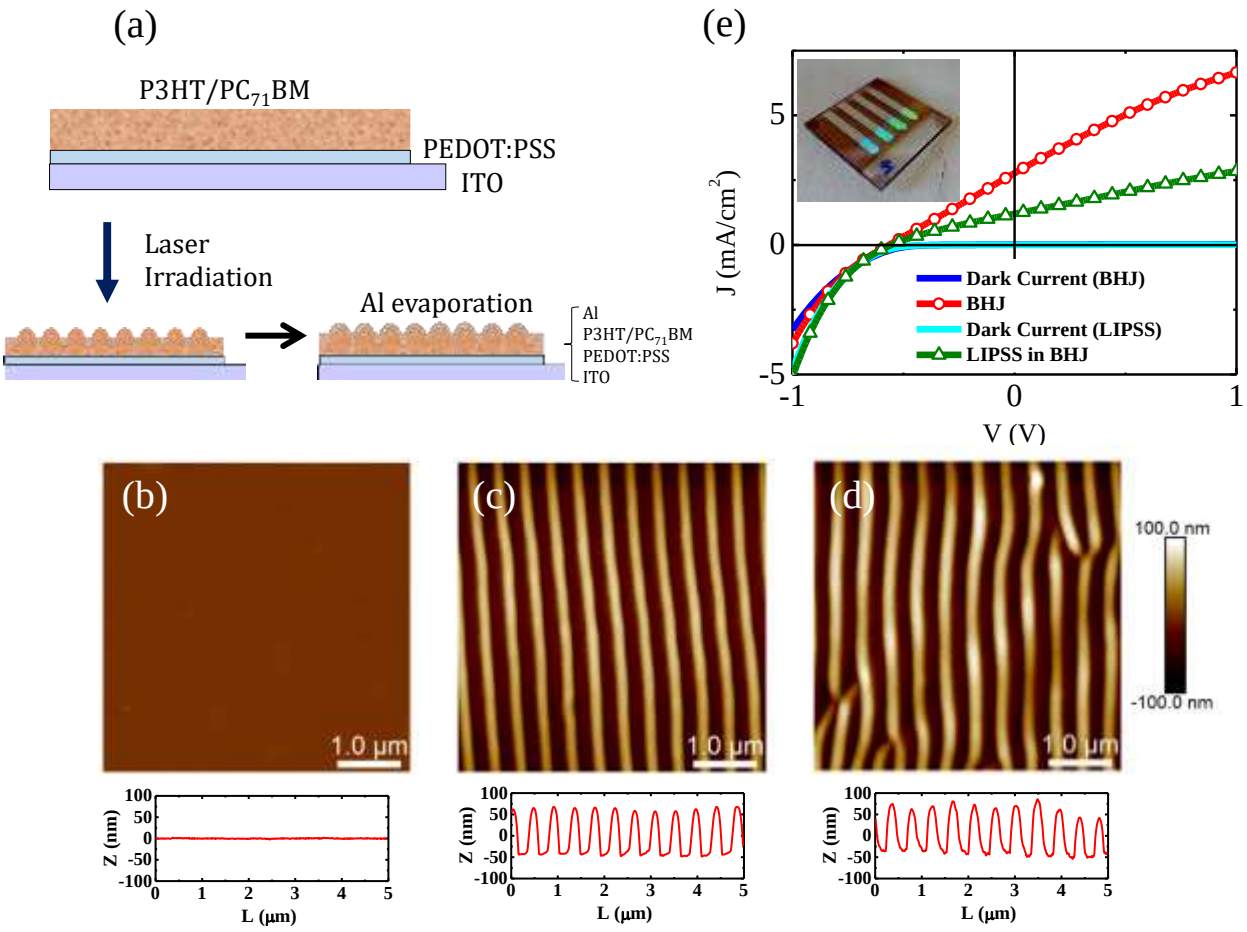

Figure 8. (a) Scheme of the bulk heterojunction architecture tested for photovoltaic characterization of P3HT:$PC_{71}BM$ systems with LIPSS. 5x5 μm^2 AFM images of the surface of the active on a BHJ solar cell: (b) before, (c) after laser irradiation and (d) after deposition of the aluminium top electrode. Height profiles are provided at the bottom of the images. (e) I-V characteristics of the LIPSS solar cell in the dark and under illumination. For the sake of comparison, data for the unstructured BHJ solar cell are also included. The inset in Fig. 8e shows the real heterojunction solar cell device exhibiting iridescence in the LIPSS zone.

In order to obtain device statistics about the performance of the LIPSS solar cells, measurements for both device architectures were performed for eight different structured solar cells and for four

reference solar cells. The results are shown in Figure 9 in terms of power conversion efficiency (PCE), fill factor (FF), short-circuit current density (J_{sc}) and open-circuit voltages (V_{oc}).

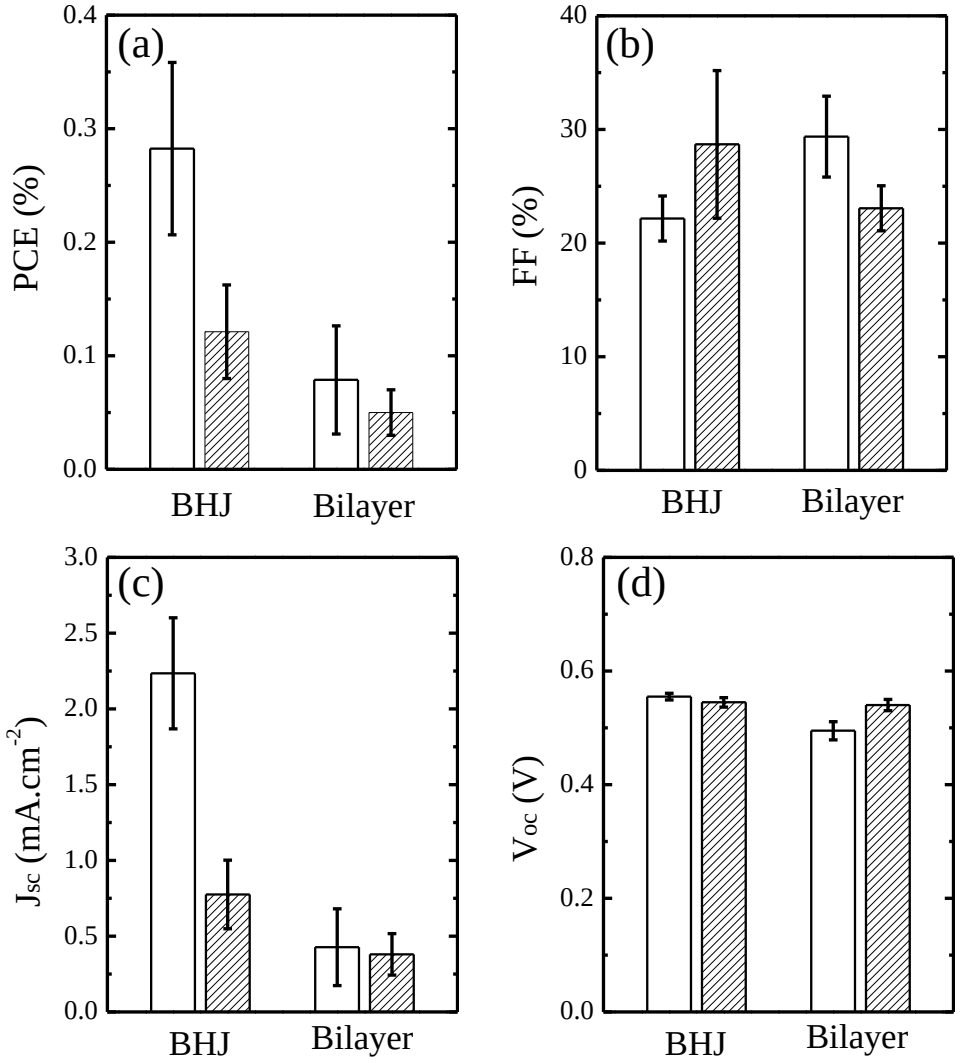

Figure 9. (a) Power conversion efficiency (PCE), (b) fill factor (FF), (c) short-circuit current density (J_{sc}) and (d) open-circuit voltages (V_{oc}) for the unstructured (non-textured bars) bilayer and bulk heterojunction (BHJ) solar cell architectures and for the corresponding ones with LIPSS (textured bars).

The performance of the solar cells with LIPSS in comparison with that of the unstructured ones is lower for the bulk heterojunction and similar for the bilayer architectures. One possible reason for that is related to the need of optimization for the presented photovoltaic systems. For the current device arrangement, according to the AFM depth profiles (Figures 7 and 8), the top-to-valley distance is comparable to the thickness of the unstructured films. Thus, after LIPSS formation, it is expected a depletion of the active layer between the PEDOT:PSS and the aluminium electrode in the valley. This effect could explain the lower performance of the LIPSS devices. Another important feature to note is that the solar cells that underwent a LIPSS structuring process have been previously laser irradiated prior to the photovoltaic characterization. Previous Raman spectroscopy results have shown that laser irradiation of P3HT provokes a decrease of the ordered-phase rather than a significant chemical degradation [36]. This effect could lead to a decrease of the electrical conductivity responsible for the decreased short-circuit current density upon LIPSS structuring. In spite of that, it is important to remark that LIPSS devices are operational as solar cells.

The FF values suggest that solar cell geometry can be optimized, although comparable values are obtained for LIPSS devices and the reference unstructured ones. As expected, the photogenerated short-circuit current of bilayer solar cells is lower than that of BHJ mainly due to the smaller donor/acceptor interface.

The V_{oc} values are similar for both LIPSS and unstructured devices. This indicates a sound preservation of the device layout and the structural integrity of the materials composing the whole layer stack. Moreover, we can see how for bilayer solar cells the V_{oc} increase by about 10%. Taking in account that the vertical profile of the imprinted structure has a height comparable to the original film thickness, it becomes remarkable that the LIPSS process means a dramatic gain in donor-

acceptor interface for bilayer devices. This enlarged interface is expected to significantly decrease the non-geminate recombination, feature which is in good agreement with the improved V_{oc}.[62, 63]. In spite of the quantitative results, our data proves that both the LIPSS P3HT: $PC_{71}BM$ bilayer system and the LIPSS P3HT:$PC_{71}BM$ blend system, preserve their photovoltaic properties for photocurrent generation. Moreover, LIPSS shows the path for device improvement upon structuring and yields improvements in FF and V_{oc} that could potentially lead to improved solar devices after optimization. This demonstrates that LIPSS can be, in principle, incorporated into organic photovoltaics technology although additional effort is necessary in order to improve the performance of the LIPSS devices. It is clear that it will be necessary to further advance in the knowledge of physico-chemical and morphological changes occurring during light exposure in order to characterize the reorganization processes that take place during irradiation. In particular, to optimize the active layer in the valleys of LIPSS devices a first approach would consist in considering thicker films with different levels of LIPSS order. In addition by using different irradiation conditions like fluence, number of pulses, laser beam polarization or combining successive irradiations with different polarization orientation [34] could be explored in order to improve performance of LIPSS solar cells. In fact, wrinkles and folds resulting from linear and nonlinear elastic instabilities have been reported to guide and retain light within the photoactive regions of photovoltaics[64].

4. CONCLUSIONS

In conclusion we have shown that laser induced periodic surface structures formation in P3HT spin-coated films takes place optimally within a certain range of thicknesses between 80 and 280 nm and for a laser irradiation fluence range between 22 and 30 mJ/cm^2. These conditions translate

well upon dealing with LIPSS formation of the photovoltaic P3HT:$PC_{71}BM$ blend on both bilayer and bulk heterogeneous solar cell architecture. Laser irradiation forming LIPSS on the surface of the active layer do not preclude the generation of electrical photocurrent by light illumination proving that LIPSS can be incorporated into organic photovoltaics. Specifically, we proved that LIPSS can be created on an active layer comprising P3HT and $PC_{71}BM$. Moreover, it is possible to prepare a LIPSS active layer between a bottom ITO electrode coated with a thin layer of (PEDOT:PSS) and a metallic top electrode. For the bilayer architecture an increase of about 10 % is observed in the V_{oc} for the LIPSS cell. Finally, the heterogeneous electrical conductivity of the P3HT LIPSS surface does not compromise the generation of photocurrent.

ACKNOWLEDGMENT

This work has been supported by Spanish Ministry of Economy under the projects CTQ 2013-43086-P, MAT2014-59187-R, and MAT2015-66443-C02-1-R. J.C. acknowledges the China Scholarship Council for funding her research (File NO. 201207040083). E.R. and A.R-R thank MINECO for the tenure of a Ramón y Cajal contract (No. RYC-2011-08069) and FPI (BES-2013-062620) contracts, respectively. P.M.-B. and D.M.G. acknowledge financial support by TUM.solar in the frame of the Bavarian Collaborative Research Project “Solar technologies go Hybrid" (SolTec), by the GreenTech Initiative (Interface Science for Photovoltaics - ISPV) of the EuroTech Universities and by the Nanosystems Initiative Munich (NIM). We thank Daniel Hermida and Wim Bras for outstanding support during beamtime in DUBBLE at ESRF. Fruitful comments of A. Urbina are gratefully acknowledged.

REFERENCES

(1) Hoppe, H.; Sariciftci, N. S., Organic Solar Cells: An Overview. *J. Mater.Res.* **2004,** *19* (7), 1924-1945.
(2) Günes, S.; Neugebauer, H.; Sariciftci, N. S., Conjugated Polymer-Based Organic Solar Cells. *Chem. Rev.* **2007,** *107* (4), 1324-1338.
(3) He, Z.; Zhong, C.; Su, S.; Xu, M.; Wu, H.; Cao, Y., Enhanced Power-Conversion Efficiency in Polymer Solar Cells Using an Inverted Device Structure. *Nat. Photonics* **2012,** *6* (9), 591-595.
(4) Su, Y. W.; Lan, S. C.; Wei, K. H., Organic Photovoltaics. *Mater. Today* **2012,** *15* (12), 554-562.
(5) Li, Z.; Wong, H. C.; Huang, Z.; Zhong, H.; Tan, C. H.; Tsoi, W. C.; Kim, J. S.; Durrant, J. R.; Cabral, J. T., Performance Enhancement of Fullerene-Based Solar Cells by Light Processing. *Nat. Commun.* **2013,** *4*, 2227.
(6) Kaur, N.; Singh, M.; Pathak, D.; Wagner, T.; Nunzi, J. M., Organic Materials for Photovoltaic Applications: Review and Mechanism. *Synth. Met.* **2014,** *190*, 20-26.
(7) Pathak, D.; Wagner, T.; Adhikari, T.; Nunzi, J. M., Photovoltaic Performance of AgInSe2-Conjugated Polymer Hybrid System Bulk Heterojunction Solar Cells. *Synth. Met.* **2015,** *199*, 87-92.
(8) Pathak, D.; Wagner, T.; Adhikari, T.; Nunzi, J. M., $AgInSe_2$.PCBM.P3HT Inorganic Organic Blends for Hybrid Bulk Heterojunction Photovoltaics. *Synth. Met.* **2015,** *200*, 102-108.
(9) Pathak, D.; Bedi, R. K.; Kaur, D.; Kumar, R., Fabrication of Densely Distributed Silver Indium Selenide Nanorods by Using Ag+ Ion Irradiation. *J. Korean Phys. Soc.* **2010,** *57* (3), 474-479.
(10) Pathak, D.; Bedi, R. K.; Kaur, D., Effect of Substrate Temperature on the Structural, Optical, and Electrical Properties of Silver-Indium-Selenide Films Prepared by Using Laser Ablation. *J. Korean Phys. Soc.* **2010,** *56* (3), 836-841.
(11) Ruderer, M. A.; Guo, S.; Meier, R.; Chiang, H.-Y.; Koerstgens, V.; Wiedersich, J.; Perlich, J.; Roth, S. V.; Müller-Buschbaum, P., Solvent-Induced Morphology in Polymer-Based Systems for Organic Photovoltaics. *Adv. Funct. Mater.* **2011,** *21* (17), 3382-3391.
(12) Ruderer, M. A.; Müller-Buschbaum, P., Morphology of Polymer-Based Bulk Heterojunction Films for Organic Photovoltaics. *Soft Matter* **2011,** *7* (12), 5482-5493.
(13) Dang, M. T.; Hirsch, L.; Wantz, G., P3HT:PCBM, Best Seller in Polymer Photovoltaic Research. *Adv. Mater.* **2011,** *23* (31), 3597-3602.
(14) Oklobia, O.; Shafai, T. S., A Quantitative Study of the Formation of PCBM Clusters Upon Thermal Annealing of P3HT/PCBM Bulk Heterojunction Solar Cell. *Sol. Energy Mater. Sol. Cells* **2013,** *117*, 1-8.
(15) Guo, S.; Ruderer, M. A.; Rawolle, M.; Körstgens, V.; Birkenstock, C.; Perlich, J.; Müller-Buschbaum, P., Evolution of Lateral Structures during the Functional Stack Build-up of P3HT:PCBM-Based Bulk Heterojunction Solar Cells. *ACS Appl. Mater. Interfaces* **2013,** *5* (17), 8581-8590.
(16) Tromholt, T.; Madsen, M. V.; Krebs, F. C., Ultra High Open Circuit Voltage (>1 V) of Poly-3-Hexylthiophene Based Organic Solar Cells With Concentrated Light. *Appl. Phys. Lett.* **2013,** *102* (12), 123904.
(17) Khelifi, S.; Voroshazi, E.; Spoltore, D.; Piersimoni, F.; Bertho, S.; Aernouts, T.; Manca, J.; Lauwaert, J.; Vrielinck, H.; Burgelman, M., Effect of Light Induced Degradation on Electrical Transport and Charge Extraction in Polythiophene:Fullerene (P3HT:PCBM) Solar Cells. *Sol. Energy Mater. Sol. Cells* **2014,** *120, Part A*, 244-252.

(18) Liu, Y.; Zhao, J.; Li, Z.; Mu, C.; Ma, W.; Hu, H.; Jiang, K.; Lin, H.; Ade, H.; Yan, H., Aggregation and Morphology Control Enables Multiple Cases of High-Efficiency Polymer Solar Cells. *Nat. Commun.* **2014,** *5*, 5293.
(19) He, Z.; Xiao, B.; Liu, F.; Wu, H.; Yang, Y.; Xiao, S.; Wang, C.; Russell, T. P.; Cao, Y., Single-Junction Polymer Solar Cells with High Efficiency and Photovoltage. *Nat. Photonics* **2015,** *9* (3), 174-179.
(20) Zhao, W.; Qian, D.; Zhang, S.; Li, S.; Inganäs, O.; Gao, F.; Hou, J., Fullerene-Free Polymer Solar Cells with over 11% Efficiency and Excellent Thermal Stability. *Adv. Mater.* **2016,** *28* (23), 4734-4739.
(21) Staniec, P. A.; Parnell, A. J.; Dunbar, A. D. F.; Yi, H.; Pearson, A. J.; Wang, T.; Hopkinson, P. E.; Kinane, C.; Dalgliesh, R. M.; Donald, A. M.; Ryan, A. J.; Iraqi, A.; Jones, R. A. L.; Lidzey, D. G., The Nanoscale Morphology of a PCDTBT: PCBM Photovoltaic Blend. *Adv. Energy Mater.* **2011,** *1* (4), 499-504.
(22) Mayer, A. C.; Scully, S. R.; Hardin, B. E.; Rowell, M. W.; McGehee, M. D., Polymer-Based Solar Cells. *Mater. Today* **2007,** *10* (11), 28-33.
(23) Zhao, K.; Hu, H.; Spada, E.; Krishnan Jagadamma, L.; Yan, B.; Abdelsamie, M.; Li, Y.; Yu, L.; Munir, R.; Li, R.; Ngongang Ndjawa, G. O.; Amassian, A., Highly Efficient Polymer Solar Cells with Printed Photoactive Layer: Rational Process Transfer from Spin-Coating. *J. Mater. Chem. A* **2016,** *DOI: 10.1039/C6TA06258J*.
(24) Jean, J.; Wang, A.; Bulović, V., In Situ Vapor-Deposited Parylene Substrates for Ultra-Thin, Lightweight Organic Solar Cells. *Org. Electron.* **2016,** *31*, 120-126.
(25) Ren, M.; Sweelssen, J.; Grossiord, N.; Gorter, H.; Eggenhuisen, T. M.; Andriessen, R., Inkjet Printing Technology for OPV Applications. *J. Imaging Sci. Technol.* **2012,** *56* (4), 40504.
(26) Fukuda, T.; Toda, A.; Takahira, K.; Suzuki, K.; Liao, Y.; Hirahara, M.; Saito, M.; Osaka, I., Molecular Ordering of Spin-Coated and Electrosprayed P3HT:PCBM Thin Films and Their Applications to Photovoltaic Cell. *Thin Solid Films* **2016,** *612*, 373-380.
(27) Na, S.-I.; Kim, S.-S.; Jo, J.; Oh, S.-H.; Kim, J.; Kim, D.-Y., Efficient Polymer Solar Cells with Surface Relief Gratings Fabricated by Simple Soft Lithography. *Adv. Funct. Mater.* **2008,** *18* (24), 3956-3963.
(28) Aryal, M.; Trivedi, K.; Hu, W. C., Nano-Confinement Induced Chain Alignment in Ordered P3HT Nanostructures Defined by Nanoimprint Lithography. *ACS Nano* **2009,** *3* (10), 3085-3090.
(29) Pfadler, T.; Coric, M.; Palumbiny, C. M.; Jakowetz, A. C.; Strunk, K.-P.; Dorman, J. A.; Ehrenreich, P.; Wang, C.; Hexemer, A.; Png, R.-Q.; Ho, P. K. H.; Müller-Buschbaum, P.; Weickert, J.; Schmidt-Mende, L., Influence of Interfacial Area on Exciton Separation and Polaron Recombination in Nanostructured Bilayer All-Polymer Solar Cells. *ACS Nano* **2014,** *8* (12), 12397-12409.
(30) Wiedemann, W.; Sims, L.; Abdellah, A.; Exner, A.; Meier, R.; Musselman, K. P.; MacManus-Driscoll, J. L.; Müller-Buschbaum, P.; Scarpa, G.; Lugli, P.; Schmidt-Mende, L., Nanostructured Interfaces in Polymer Solar Cells. *Appl. Phys. Lett.* **2010,** *96* (26), 263109.
(31) Chen, D.; Zhao, W.; Russell, T. P., P3HT Nanopillars for Organic Photovoltaic Devices Nanoimprinted by AAO Templates. *ACS Nano* **2012,** *6* (2), 1479-1485.
(32) Sarkar, K.; Schaffer, C. J.; Gonzalez, D. M.; Naumann, A.; Perlich, J.; Müller-Buschbaum, P., Tuning the Pore Size of ZnO Nano-Grids Via Time-Dependent Solvent Annealing. *J. Mater. Chem. A* **2014,** *2* (19), 6945-6951.

(33) Meier, R.; Birkenstock, C.; Palumbiny, C. M.; Müller-Buschbaum, P., Efficiency-Improved Organic Solar Cells Based on Plasticizer Assisted Soft Embossed PEDOT:PSS Layers. *Phys. Chem. Chem. Phys.* **2012,** *14* (43), 15088-15098.
(34) Rebollar, E.; Castillejo, M.; Ezquerra, T. A., Laser Induced Periodic Surface Structures on Polymer Films: From Fundamentals to Applications. *Eur. Polym. J.* **2015,** *73*, 162-174.
(35) Guosheng, Z.; Fauchet, P. M.; Siegman, A. E., Growth of Spontaneous Periodic Surface Structures on Solids During Laser Illumination *Phys. Rev. B* **1982,** *26* (10), 5366-5381.
(36) Rodriguez-Rodriguez, A.; Rebollar, E.; Soccio, M.; Ezquerra, T. A.; Rueda, D. R.; Vicente Garcia-Ramos, J.; Castillejo, M.; Garcia-Gutierrez, M.-C., Laser-Induced Periodic Surface Structures on Conjugated Polymers: Poly(3-hexylthiophene). *Macromolecules* **2015,** *48* (12), 4024-4031.
(37) Rebollar, E.; Pérez, S.; Hernández, J. J.; Martín-Fabiani, I.; Rueda, D. R.; Ezquerra, T. A.; Castillejo, M., Assessment and Formation Mechanism of Laser-Induced Periodic Surface Structures on Polymer Spin-Coated Films in Real and Reciprocal Space. *Langmuir* **2011,** *27* (9), 5596-5606.
(38) Rebollar, E.; Vazquez de Aldana, J. R.; Perez-Hernandez, J. A.; Ezquerra, T. A.; Moreno, P.; Castillejo, M., Ultraviolet and Infrared Femtosecond Laser Induced Periodic Surface Structures on Thin Polymer Films. *Appl. Phys. Lett.* **2012,** *100* (4), 041106.
(39) Zhou, H.; Yang, L.; You, W., Rational Design of High Performance Conjugated Polymers for Organic Solar Cells. *Macromolecules* **2012,** *45* (2), 607-632.
(40) Garcia-Valverde, R.; Cherni, J. A.; Urbina, A., Life Cycle Analysis of Organic Photovoltaic Technologies. *Prog. Photovoltaics* **2010,** *18* (7), 535-558.
(41) Cui, J.; Martínez-Tong, D. E.; Sanz, A.; Ezquerra, T. A.; Rebollar, E.; Nogales, A., Relaxation and Conductivity in P3HT/PC71BM Blends As Revealed by Dielectric Spectroscopy. *Macromolecules* **2016,** *49* (7), 2709-2717.
(42) Bras, W.; Dolbnya, I. P.; Detollenaere, D.; van Tol, R.; Malfois, M.; Greaves, G. N.; Ryan, A. J.; Heeley, E., Recent Experiments on a Combined Small-Angle/Wide-Angle X-Ray Scattering Beam Line at the ESRF. *J. Appl. Crystallogr.* **2003,** *36*, 791-794.
(43) Hammersley, A., *http://www.esrf.eu/computing/scientific/FIT2D/*. 2004.
(44) Schubert, D. W., Spin Coating as a Method for Polymer Molecular Weight Determination. *Polym. Bull.* **1997,** *38* (2), 177-184.
(45) Chang, C.-C.; Pai, C.-L.; Chen, W.-C.; Jenekhe, S. A., Spin Coating of Conjugated Polymers for Electronic and Optoelectronic Applications. *Thin Solid Films* **2005,** *479* (1–2), 254-260.
(46) Ruderer, M. A.; Metwalli, E.; Wang, W.; Kaune, G.; Roth, S. V.; Müller-Buschbaum, P., Thin Films of Photoactive Polymer Blends. *ChemPhysChem* **2009,** *10* (4), 664-671.
(47) Rodriguez-Rodriguez, A.; Soccio, M.; Martinez-Tong, D. E.; Ezquerra, T. A.; Watts, B.; Garcia-Gutierrez, M.-C., Competition Between Phase Separation and Structure Confinement in P3HT/PCDTBT Heterojunctions: Influence on Nanoscale Charge Transport. *Polymer* **2015,** *77*, 70-78.
(48) Kohn, P.; Hüttner, S.; Komber, H.; Senkovskyy, V.; Tkachov, R.; Kiriy, A.; Friend, R. H.; Steiner, U.; Huck, W. T. S.; Sommer, J.-U.; Sommer, M., On the Role of Single Regiodefects and Polydispersity in Regioregular Poly(3-hexylthiophene): Defect Distribution, Synthesis of Defect-Free Chains, and a Simple Model for the Determination of Crystallinity. *J. Am. Chem. Soc.* **2012,** *134* (10), 4790-4805.

(49) Martín-Fabiani, I.; Rebollar, E.; Pérez, S.; Rueda, D. R.; García-Gutiérrez, M. C.; Szymczyk, A.; Roslaniec, Z.; Castillejo, M.; Ezquerra, T. A., Laser-Induced Periodic Surface Structures Nanofabricated on Poly(trimethylene terephthalate) Spin-Coated Films. *Langmuir* **2012,** *28* (20), 7938-7945.
(50) Cui, J.; Nogales, A.; Ezquerra, T. A.; Rebollar, E., Influence of Substrate and Film Thickness on Polymer LIPSS Formation. *Appl. Surf. Sci.* **2017,** *394*, 125-131.
(51) Fardel, R.; Nagel, M.; Lippert, T.; Nuesch, F.; Wokaun, A.; Luk'yanchuk, B. S., Influence of Thermal Diffusion on The Laser Ablation of Thin Polymer Films. *Appl. Phys. A-Mater. Sci. Process.* **2008,** *90* (4), 661-667.
(52) Rueda, D. R.; Martin-Fabiani, I.; Soccio, M.; Alayo, N.; Perez-Murano, F.; Rebollar, E.; Garcia-Gutierrez, M. C.; Castillejo, M.; Ezquerra, T. A., Grazing-Incidence Small-Angle X-Ray Scattering of Soft and Hard Nanofabricated Gratings. *J. Appl. Crystallogr.* **2012,** *45*, 1038-1045.
(53) Bolognesi, A.; Porzio, W.; Provasoli, F.; Ezquerra, T., The Thermal Behavior of Low-Molecular Weight Poly(3-decylthiophene). *Makromol. Chem.* **1993,** *194* (3), 817-827.
(54) Bolognesi, A.; Porzio, W.; Zhuo, G.; Ezquerra, T., The Thermal Behaviour of Poly(3-octylthienylene) Synthesized by an Ni-Based Catalyst: DSC, Optical Microscopy and XRD Analyses. *Eur. Polym. J.* **1996,** *32* (9), 1097-1103.
(55) Baker, J. L.; Jimison, L. H.; Mannsfeld, S.; Volkman, S.; Yin, S.; Subramanian, V.; Salleo, A.; Alivisatos, A. P.; Toney, M. F., Quantification of Thin Film Crystallographic Orientation Using X-ray Diffraction with an Area Detector. *Langmuir* **2010,** *26* (11), 9146-9151.
(56) DeLongchamp, D. M.; Kline, R. J.; Herzing, A., Nanoscale Structure Measurements for Polymer-Fullerene Photovoltaics. *Energy Environ. Sci.* **2012,** *5* (3), 5980-5993.
(57) Jiang, Z., GIXSGUI: a MATLAB Toolbox for Grazing-Incidence X-Ray Scattering Data Visualization and Reduction, and Indexing of Buried Three-Dimensional Periodic Nanostructured Films. *J. Appl. Crystallogr.* **2015,** *48*, 917-926.
(58) Wu, Z.; Petzold, A.; Henze, T.; Thurn-Albrecht, T.; Lohwasser, R. H.; Sommer, M.; Thelakkat, M., Temperature and Molecular Weight Dependent Hierarchical Equilibrium Structures in Semiconducting Poly(3-hexylthiophene). *Macromolecules* **2010,** *43* (10), 4646-4653.
(59) Kohn, P.; Rong, Z.; Scherer, K. H.; Sepe, A.; Sommer, M.; Müller-Buschbaum, P.; Friend, R. H.; Steiner, U.; Hüttner, S., Crystallization-Induced 10-nm Structure Formation in P3HT/PCBM Blends. *Macromolecules* **2013,** *46* (10), 4002-4013.
(60) Capitan, M. J.; Rueda, D. R.; Ezquerra, T. A., Inhibition of the Crystallization in Nanofilms of Poly(3-hydroxybutyrate). *Macromolecules* **2004,** *37* (15), 5653-5659.
(61) Ma, Y.; Hu, W.; Reiter, G., Lamellar Crystal Orientations Biased by Crystallization Kinetics in Polymer Thin Films. *Macromolecules* **2006,** *39* (15), 5159-5164.
(62) Foertig, A.; Wagenpfahl, A.; Gerbich, T.; Cheyns, D.; Dyakonov, V.; Deibel, C., Nongeminate Recombination in Planar and Bulk Heterojunction Organic Solar Cells. *Adv. Energy Mater.* **2012,** *2* (12), 1483-1489.
(63) Garcia-Belmonte, G.; Boix, P. P.; Bisquert, J.; Sessolo, M.; Bolink, H. J., Simultaneous Determination of Carrier Lifetime and Electron Density-of-States in P3HT:PCBM Organic Solar Cells Under Illumination by Impedance Spectroscopy. *Sol. Energy Mater. Sol. Cells* **2010,** *94* (2), 366-375.
(64) Kim, J. B.; Kim, P.; Pegard, N. C.; Oh, S. J.; Kagan, C. R.; Fleischer, J. W.; Stone, H. A.; Loo, Y.-L., Wrinkles and Deep Folds as Photonic Structures in Photovoltaics. *Nat. Photonics* **2012,** *6* (5), 327-332.

TOC

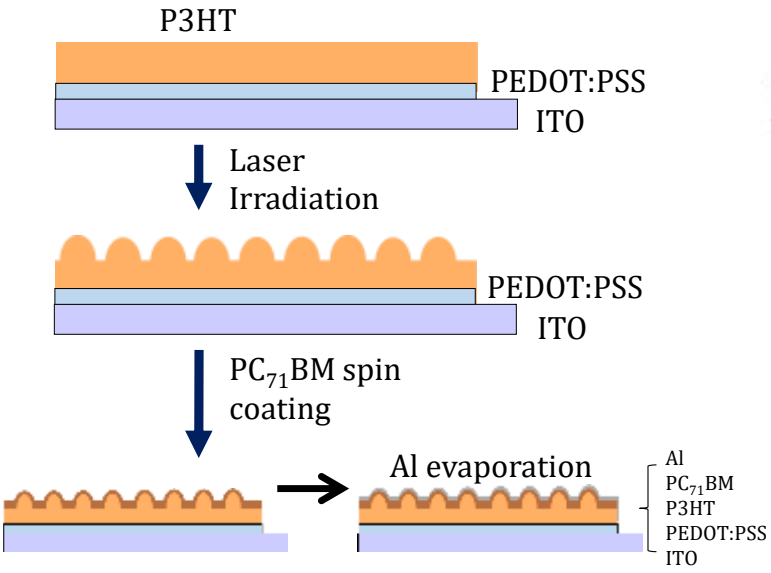
P3HT
PEDOT:PSS
ITO
Laser
Irradiation
PEDOT:PSS
ITO
PC71BM spin
coating
Al evaporation
Al
PC71BM
P3HT
PEDOT:PSS
ITO

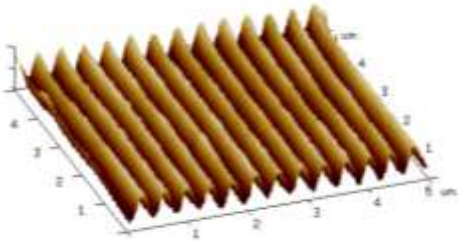


Al
LIPSS
ITO